

Fast quantum logic gates with trapped-ion qubits

V. M. Schäfer, C. J. Ballance, K. Thirumalai, L. J. Stephenson,

T. G. Ballance, A. M. Steane and D. M. Lucas

Department of Physics, University of Oxford,

Clarendon Laboratory, Parks Road, Oxford OX1 3PU, U.K.

(Dated: 14 Nov 2017)

Quantum bits based on individual trapped atomic ions constitute a promising technology for building a quantum computer¹, with all the elementary operations having been achieved with the necessary precision for some error-correction schemes²⁻⁴. However, the essential two-qubit logic gate used for generating quantum entanglement has hitherto always been performed in an adiabatic regime, where the gate is slow compared with the characteristic motional frequencies of ions in the trap³⁻⁷, giving logic speeds of order 10 kHz. There have been numerous proposals for performing gates faster than this natural “speed limit” of the trap⁸⁻¹². We implement the method of Steane *et al.*¹¹, which uses tailored laser pulses: these are shaped on 10 ns timescales to drive the ions’ motion along trajectories designed such that the gate operation is insensitive to optical phase fluctuations. This permits fast (MHz-rate) quantum logic which is robust to this important source of experimental error. We demonstrate entanglement generation for gate times as short as 480 ns; this is less than a single oscillation period of an ion in the trap, and 8 orders of magnitude shorter than the memory coherence time measured in similar calcium-43 hyperfine qubits. The method’s power is most evident at intermediate timescales, where it yields a gate error more than ten times lower than conventional techniques; for example, we achieve a 1.6 μ s gate with fidelity 99.8%. Still faster gates are possible at the price of higher laser intensity. The method requires only a single amplitude-shaped pulse and one pair of beams derived from a continuous-wave laser, and offers the prospect of combining the unrivalled coherence properties^{2,13,14}, operation fidelities²⁻⁴ and optical connectivity¹⁵ of trapped-ion qubits with the sub-microsecond logic speeds usually associated with solid state devices^{16,17}.

Deterministic entanglement of multiple qubits, an essential pre-requisite for general quantum information processing, was first achieved nearly twenty years ago using laser manipulation of qubits stored in the hyperfine ground states of trapped atomic ions⁵. Since then technical progress, the development of more robust methods, and improved understanding of error sources have yielded a steady improvement in the precision of the fundamental two-qubit quantum logic gate, with the gate error ϵ_g falling by approximately a factor of two every two years, to reach the level $\epsilon_g \approx 0.1\%$ in recent experiments^{3,4}. All elementary single-qubit operations have also been demonstrated with errors $< 0.1\%^{2-4}$. These error levels are already an order of magnitude below the threshold level required for fault-tolerant quantum error correction schemes¹⁸. In contrast the two-qubit gate speed has remained fairly constant since the first demonstrations; the gates with the lowest reported errors had durations of $30 \mu\text{s}$ and $100 \mu\text{s}$. For qubits based on solid state platforms, the interactions are much stronger, allowing significantly faster two-qubit operations (typically $\sim 50 \text{ ns}$ for superconducting circuits¹⁶, and 480 ns for the recently-demonstrated gate in silicon-based qubits¹⁷), but also leading to much shorter qubit coherence times (typically $T_2^* \sim 100 \mu\text{s}$, compared with $T_2^* \sim 1 \text{ minute}$ for atomic systems). Substantial progress has also been made in demonstrating simple algorithms and quantum simulations involving ~ 10 qubits, and in developing technologies amenable to scaling to larger numbers of qubits^{19,20}.

In previous trapped-ion work the speed of the two-qubit gate operation has been limited by the use of methods that operate in an adiabatic regime with respect to the secular motional frequencies of the ions; as these are typically $\sim 1 \text{ MHz}$, gate durations are generally $\gg 1 \mu\text{s}$, and attempts to increase the gate speed have resulted in larger gate errors (for example, $\epsilon_g = 3\%$ at the shortest reported gate time of $t_g = 5.3 \mu\text{s}$ ⁴²). With recent progress in demonstrating faster techniques of ground-state laser cooling²¹, ion shuttling^{22,23}, and qubit readout²⁴, present two-qubit gate speeds threaten to be the limiting factor in the clock speed of a trapped-ion processor based on a “quantum CCD” architecture¹, especially given that error-correction circuits typically contain more gates than state preparation and readout operations. The two-dimensional QCCD architecture would be a natural choice for implementing surface-code error correction methods¹⁸, although these can also be mapped onto one-dimensional ion chains. Errors due to ambient heating of the ions’ motion are proportional to t_g and will thus be suppressed for fast gates, which is advantageous for microfabricated traps where the ions are confined near to electrode surfaces and hence

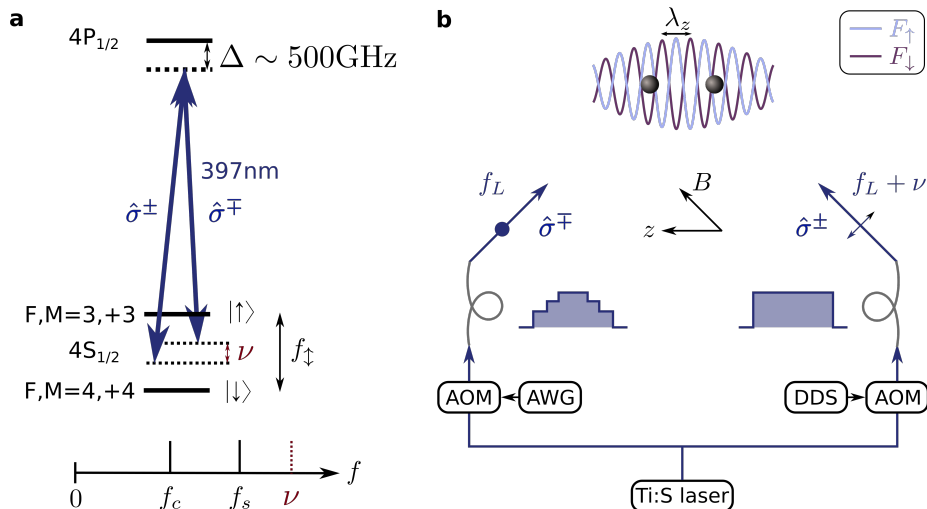


FIG. 1. Qubit states and Raman beam geometry. (a) Qubits are stored in $^{43}\text{Ca}^+$ hyperfine states $|\downarrow\rangle=4S_{1/2}^{4,+4}$ and $|\uparrow\rangle=4S_{1/2}^{3,+3}$, with separation $f_{\uparrow} = 2.87$ GHz. Ion axial motional frequencies are $(f_c, f_s = 1.92, 3.33$ MHz). The Raman beam difference frequency $\nu = 3.43f_c$ for the fastest gate, while $f_c < \nu < f_s$ for the highest-fidelity gates. (b) One Raman beam propagates parallel to the quantization axis, set by a magnetic field $B \approx 14.6$ mT. The beams are perpendicular, such that their difference k -vector is parallel to the trap axis z , and have ≈ 35 μm waists at the ions, powers of up to 200 mW, and orthogonal linear polarizations. Their interference creates a polarization “travelling standing wave” (period $\lambda_z \approx 397$ nm/ $\sqrt{2}$) that induces a spin-dependent force $F_{\downarrow}, F_{\uparrow}$ on the ions. High-bandwidth acousto-optic modulators (AOMs) shape the laser pulses on ~ 10 ns timescales; we use a constant-amplitude pulse for one beam, and an amplitude-shaped pulse for the other beam.

subject to greater electric field noise²⁵. Spin-dephasing errors due to, e.g., magnetic field fluctuations (which typically have a $1/f$ noise spectrum), will likewise be reduced, allowing the use of qubit states which have first-order sensitivity to magnetic field²⁶ (at least during gate operations, as here).

The “speed limit” set by the trap frequency f_c is not a fundamental barrier: the Coulomb interaction responsible for coupling the ions is almost instantaneous at the typical separation of trapped ions (3.5 μm in our work), and there have been a variety of theoretical proposals for fast gates with $t_g \lesssim 1/f_c$, for example refs.^{8–12}. None of these has so far been demonstrated⁴³. Here, after first exploring the limits of the conventional $\sigma_z \otimes \sigma_z$ gate mechanism

originally demonstrated by Leibfried *et al.*⁶, we implement the scheme proposed by Steane *et al.*¹¹, in which the single rectangular laser pulse used in the conventional adiabatic method is replaced by a pulse whose amplitude is shaped in time.

The operation of the gate relies on a qubit-state-dependent force, which originates from the spatially-varying light shift caused by a “travelling standing wave”, generated by the optical interference pattern of two non-copropagating laser beams with difference frequency ν (fig. 1). We specialize to the case of two ions with the force coupling only to the axial modes of motion. We discuss the behaviour in three regimes: (1) a single rectangular pulse in the adiabatic regime, (2) a single rectangular pulse in the non-adiabatic regime, (3) a fast shaped pulse or pulses.

Case 1. By choosing $\nu = f_c + \delta$ with $\delta \ll f_c$, only the centre-of-mass normal mode at frequency f_c is excited (to first approximation) and the rotating wave approximation holds for the treatment of the motion. Starting from a state cooled to the Lamb-Dicke regime ($\eta^2 n \ll 1$, where η is the Lamb-Dicke parameter and n the motional quantum number), the motion traces out an approximately circular path in the (rotating frame) phase space of the harmonic oscillator, returning to its starting point after time $t_g = 1/\delta$ (fig. 2). The geometric gate phase Φ is determined by the (signed) area enclosed by this path, which is proportional to Ω^2 , where Ω is the Rabi frequency. We require $\Phi = \pi/2$ to generate the maximally-entangled state $(|\downarrow\downarrow\rangle + i|\downarrow\uparrow\rangle + i|\uparrow\downarrow\rangle + |\uparrow\uparrow\rangle)/2$ from the separable state $(|\downarrow\downarrow\rangle + |\downarrow\uparrow\rangle + |\uparrow\downarrow\rangle + |\uparrow\uparrow\rangle)/2$ after time t_g . The gate phase Φ is independent of both the initial motional state (within the Lamb-Dicke regime), and the phase ϕ_0 of the optical beat note at the start time $t = 0$. The latter is crucial for achieving high gate fidelity in the laboratory, because ϕ_0 is sensitive to nanometre-scale length differences between the two laser beam paths. Such gates were implemented previously^{3,6}.

Case 2. The gate speed is increased by increasing δ , but for $\delta \sim f_c$ there are three complicating factors: firstly, both the centre-of-mass mode and the stretch mode (at $f_s = f_c\sqrt{3}$) of a two-ion crystal will be excited and the associated trajectories in phase space will not in general close at the same time; secondly the trajectories depend on ϕ_0 ; thirdly there is a time-dependent light shift independent of the motion but which also depends on ϕ_0 and can result in a large single-qubit phase ϕ_{LS} . Consequently the expected gate error has a complicated dependence on gate time, and rises steeply as the gate time approaches the period of the motion. This is shown in fig. 3a, together with a selection of results achieved

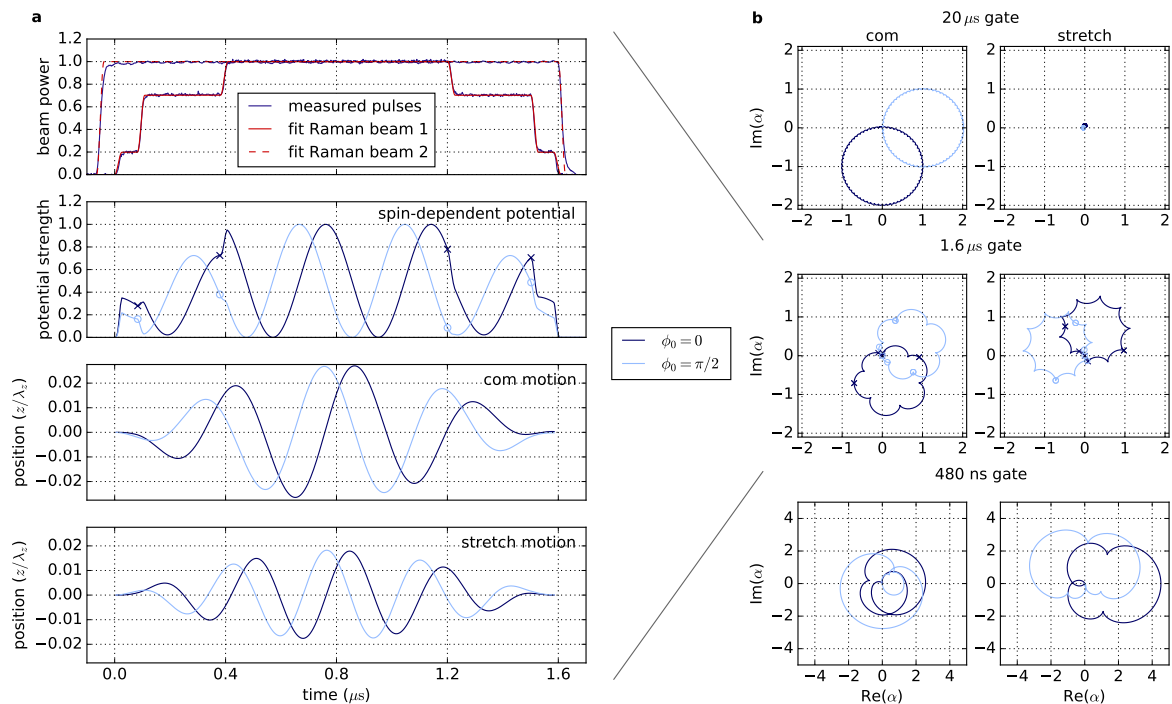


FIG. 2. Optical beat notes and motional trajectories of the ions, for two example initial optical phases $\phi_0 = (0, \pi/2)$ rad. (a) For the $t_g = 1.6 \mu\text{s}$ gate the plots show, from top: the Raman laser pulses; their (calculated) optical beat note, which gives rise to the spin- and position-dependent potential (and hence force) that the ions experience; the ions' centre-of-mass displacement; their stretch-mode displacement. The beat frequency is $\nu = 2.63 \text{ MHz} \approx 1.37 f_c$. The force and motions clearly depend on ϕ_0 ; however, the pulse shape is designed such that, for all ϕ_0 , both trajectories return to zero displacement at $t = t_g$. (b) Phase-space trajectories (rotating frame) for gates in three regimes. For a conventional adiabatic ($t_g = 20 \mu\text{s}$) gate, $\nu \approx 1.03 f_c$ and the stretch mode is barely excited; ϕ_0 affects the orientation of the (nearly-circular) trajectory, but not its shape or area. For $t_g = 1.6 \mu\text{s}$, both modes are driven and ϕ_0 affects the shape of the trajectories slightly; amplitude shaping is necessary to close the loops for both modes and to ensure the net gate phase is independent of ϕ_0 . (Symbols correspond to steps in the pulse amplitude.) For $t_g = 480 \text{ ns} < 1/f_c$ the trajectory depends strongly on ϕ_0 ; this illustration makes the Lamb-Dicke approximation, but out-of-Lamb-Dicke effects mean that the loops no longer close, leading to significant gate errors.

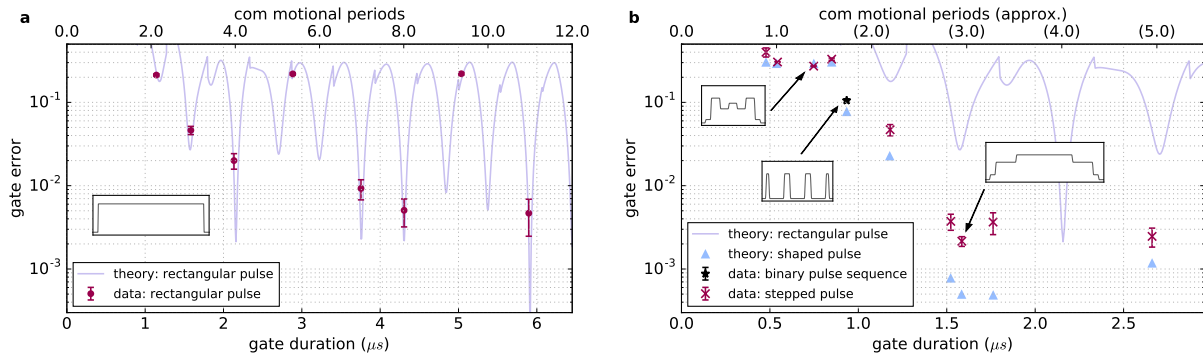


FIG. 3. Theoretical and experimental two-qubit gate errors (error bars give 1σ statistical errors). (a) Conventional single rectangular pulse. The curve shows the coherent error achievable (i.e. excluding photon scattering and technical errors). At each time, Ω and ν are adjusted to minimize ϵ_g ; discontinuities occur where the optimum ν switches between $f_c < \nu < f_s$ and $\nu > f_s$. (Although significant reduction in gate error can be made by shaping the pulse edges³ when $t_g \gg 1/f_c$, negligible improvement is possible when the gate duration becomes comparable to the shaping time constant, at $t_g \lesssim 4.5/f_c$.) Data points show experimentally-measured gate errors. (b) Amplitude-shaped pulses. The curve is repeated from (a) for comparison. Simulated errors (triangles) are dominated by out-of-Lamb-Dicke effects for $t_g < 1.5 \mu\text{s}$. The other points are measured gate errors, after optimizing pulse-shape parameters using real-time feedback from the experiment. Insets illustrate example pulse shapes.

in our experiments. We measure a gate error $\epsilon_g = 2.0(5)\%$ for $t_g = 2.13 \mu\text{s}$, and the theory shows that no solutions exist with errors below this at shorter times.

Case 3. Replacing the single rectangular pulse of the conventional method by a shaped pulse gives more degrees of freedom (i.e. those parameters describing the pulse shape), which can be exploited to find especially well-performing or “magic” pulses. In particular, we want to achieve all of the following: that the phase space trajectories for both modes should close simultaneously at $t = t_g$; that the appropriate sum of (signed) areas enclosed be independent of ϕ_0 , even though the trajectories themselves may depend on ϕ_0 ; that the light-shift induced phase ϕ_{LS} be independent of ϕ_0 and preferably small; that the pulse area is small to minimize photon scattering²⁷ and that the gate error be not too sensitive to errors in parameter settings. A shaped pulse or pulse-sequence is deemed a ‘solution’ when it has all these properties, such that the gate error predicted for a perfectly realized sequence is

below an upper bound ϵ_t set by practical considerations. That is, one sets ϵ_t well below the error one is prepared to accept in the laboratory, and seeks solutions by numerical search.

Several classes of solution are given by Steane *et al.* for particularly simple pulse shapes. We implemented two types of time-symmetric sequence: a binary pulse sequence (where a constant amplitude force is simply switched on and off), and five- or seven-segment “stepped” pulses. Example phase-space trajectories are shown in fig. 2. By this means we obtained gates up to an order of magnitude faster than those previously demonstrated. However, to understand the experimentally observed gate error, and the optimal pulse shapes, we had to develop the theory further.

The solutions given in ref.¹¹ assume that the motion remains within the Lamb-Dicke regime; for $t_g \sim 1/f_c$ this is a poor approximation, as large excursions in phase space are required to enclose sufficient area. For large excursions, the ions become sensitive to the spatial variation of the force, leading to modification of the trajectories and squeezing of the motional wavepackets²⁸. We extended the theory with numerical modelling to include the effects of motional excursion beyond the Lamb-Dicke regime, and found solutions which give the minimum gate error for times in the range $200 \text{ ns} < t_g < 5.0 \mu\text{s}$ (see Methods). The most efficient solutions, giving optimal use of the available laser power, are found when $f_c < \nu < f_s$, where both modes are excited such that the geometric phases from each mode add constructively ($\Phi = \Phi_c + \Phi_s$); conversely, when $\nu > f_s$, the phases subtract and more laser power is required to achieve $\Phi = \pi/2$ (in turn leading to higher photon scattering error²⁷). The numerically-calculated errors for some of these efficient solutions are shown in fig.3b, together with experimentally achieved gate errors for gate times between 480 ns and $2.7 \mu\text{s}$ (see Methods for experimental details). The fastest gate time is slightly below the centre-of-mass motional period ($1/f_c = 540 \text{ ns}$), but the error is large (40%). The binary pulse sequence achieves 11% error at $0.93 \mu\text{s}$ gate time. The minimum error measured is 0.22(3)% at $t_g = 1.6 \mu\text{s}$, using a stepped pulse, which is close to the lowest two-qubit gate errors previously reported^{3,4}, whilst being 20–60 times faster. This error is an order of magnitude lower than that achievable with the conventional single-pulse method at the same t_g . For the $1.6 \mu\text{s}$ gate, we estimate the total error due to known sources to be $\approx 0.18\%$ (Table I).

In our setup the gate speed and fidelity are limited by the breakdown of the Lamb-Dicke approximation for $t_g \lesssim 1/f_c$. Faster and/or higher fidelity gates are possible by reducing the

error source	$t_g = 1.6 \mu\text{s}$	$t_g = 480 \text{ ns}$
out-of-Lamb-Dicke effects	5×10^{-4}	3×10^{-1}
optical phase chirp	$\sim 4 \times 10^{-4}$	$\sim 6 \times 10^{-3}$
pulse timing and amplitudes	$\sim 2 \times 10^{-4}$	$\sim 1 \times 10^{-3}$
radial mode excitation	$\lesssim 4 \times 10^{-5}$	$\lesssim 4 \times 10^{-3}$
photon scattering	6×10^{-4}	7×10^{-3}
centre-of-mass heating rate	8×10^{-5}	3×10^{-5}
total error	1.8×10^{-3}	3.3×10^{-1}

TABLE I. Error budget for the highest-fidelity and fastest gates achieved. The total is the linear sum of the individual errors; this assumes they are constant and add incoherently.

Lamb-Dicke parameters (here $\eta_c = 0.126$, $\eta_s = 0.096$); for example, decreasing the 90° angle between the two laser beams (fig. 1b) to give $\eta_c = 0.08$ would reduce the error contribution from out-of-Lamb-Dicke effects to 7×10^{-5} . This in turn requires higher laser intensities at the ions; although we use a moderately high laser power ($\sim 150 \text{ mW}$ per beam for the fastest gate), the intensity is modest ($\sim 0.1 \text{ mW}/\mu\text{m}^2$) and the spot size ($w_0 \approx 35 \mu\text{m}$) could be significantly reduced. Alternatively, if the optical phase ϕ_0 could be sufficiently well controlled, solutions can be found for fixed ϕ_0 which allow faster gates and higher fidelities¹².

In conclusion, we have demonstrated a fast ($1.6 \mu\text{s}$), robust two-qubit gate method for trapped-ion qubits which combines state-of-the-art gate fidelity (99.8%) with more than an order of magnitude increase in gate speed. At the fastest speed demonstrated (480 ns) the fidelity achieved (60%) may not be useful for information processing, but might have other applications (such as quantum logic spectroscopy of short-lived exotic species^{29,30}; this would also require the use of fast laser cooling techniques³¹). The method is technically simple, requiring only a single amplitude-shaped pulse from a cw laser, and the laser intensities required are within reach of miniature solid state violet diodes³². These considerations are important if the techniques are ultimately to be scaled to the very large numbers of qubits necessary for an error-corrected quantum computer.

METHODS

Numerical modelling

Most trapped-ion experiments can be described in the Lamb-Dicke regime, i.e. the optical field is assumed to be uniform over the extent of each ion's wavefunction. However for the large phase-space displacements necessary to perform fast gates this assumption breaks down: the curvature of the field can no longer be neglected. This means the force experienced by an ion depends on its displacement in phase space and this leads to squeezing of the wavefunction, as well as modification of the motional trajectory.

To model the coherent error of a given gate sequence, we therefore numerically integrate the full Hamiltonian (that is, without making the Lamb-Dicke approximation) using the split-operator method, explicitly averaging over different initial optical phases. As this is a computationally intensive process, the gate sequences used in the experiments were pre-selected by an efficient solver that works in the Lamb-Dicke regime. Following Steane *et al.*, we optimize candidate solutions starting from a random seed, and select a set of candidate solutions that have an error of $< 10^{-4}$ in the Lamb-Dicke approximation.

These candidate solutions were then evaluated using the full solver, and the most promising were optimized further. For the experiments, we chose solutions from this set by looking for a combination of low coherent error and low integrated pulse area (this both selects for a low photon scattering error²⁷, and avoids fragile sequences that use large motional excitations, which are more sensitive to parameter variations).

Several different pulse shapes were evaluated. The seven-segment symmetric pulse shape offered a sufficient number of parameters to find a dense set of good solutions, whilst being easy to implement and to verify. The exact shape of the rising and falling edges is unimportant: the rise-time can be varied from zero to the segment length without a change in gate fidelity, providing that an overall scaling factor is applied to the gate Rabi frequency to compensate for the changing spectral content.

Raman beams

The light source for the Raman beams is a frequency-doubled Ti:sapphire laser with 1.8W output power at 397 nm³³. The Raman detuning was $\Delta = -1$ THz for single rectangular

pulses; for shaped-pulse gates with $t_g \leq 1 \mu\text{s}$, $\Delta = -200 \text{ GHz}$ and for $t_g > 1 \mu\text{s}$, $\Delta = -800 \text{ GHz}$. The detuning was changed to reduce photon scattering errors for gates requiring lower Rabi frequencies. For the fastest gate, peak powers of 192 mW and 96 mW were used for the two Raman beams, which had waists at the ions of $33 \mu\text{m}$ and $38 \mu\text{m}$ respectively ($1/e^2$ intensity radius). The ratios of Raman beam powers were chosen such that the scattering error was approximately minimized. The beams were modulated by a pair of acousto-optic modulators³⁴ (AOMs) with 24 ns rise time (10%–90%) to create the shaped pulses driving the gate. The amplitude-shaped radiofrequency (RF, 200 MHz) signal for the stepped pulse was defined with an arbitrary waveform generator³⁵ (AWG) and fed to the first AOM. The second AOM was driven by a direct digital synthesis (DDS) source³⁶ (fig. 1b).

Phase chirps of the modulated beam were measured in an optical homodyne experiment and found to be significant during switching of the RF amplitude. Driving the AOM at its centre frequency (200 MHz) minimized the phase chirps³⁷ such that their contribution to the gate error was small (table I).

Pulse calibration

Performing fast gates with high fidelities requires precise control of the pulse parameters. Due to the non-linear response of the AOM for different RF drive amplitudes, the pulse shape was measured on a photodiode and the relative drive amplitudes of each pulse segment were adjusted to match the measured amplitudes to their theoretically-predicted optimum levels. The relative amplitudes of the stepped pulses were set with $\pm 0.2\%$ accuracy. The waveform programmed into the 1.25 Gsps AWG had a 5.0 ns risetime in order to spread the pulse edges over several time points and improve the effective timing resolution. The timing precision of the optical pulses was measured to be 0.2 ns (standard deviation of fitted pulse lengths). Setting the pulse-shape parameters to their theoretically-predicted values yielded optimal fidelity for all gate sequences where the Lamb-Dicke approximation held well. There are three remaining parameters characterising the gate sequence: the peak beam power, the Raman beat note frequency ν and the phase offset $\phi_{\pi/2}$ of the last $\pi/2$ -pulse of the Ramsey interferometer ($\phi_{\pi/2}$ compensates for the single-qubit phase acquired during the gate). The beat note frequency and beam power were set to their theoretically-predicted values and then optimized empirically; in all cases the optimized values agreed well with their theoretical

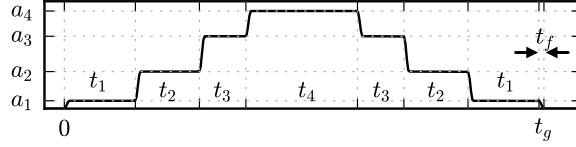
predictions. The peak pulse powers of each beam were stabilized at the beginning of each experimental sequence. The phase offset $\phi_{\pi/2}$ was calibrated empirically. Initially gate parameters were optimized with a Nelder-Mead algorithm. After the minimisation of optical phase chirps this was no longer necessary and linear optimisation of single parameters was found to be sufficient. A list of parameters for the fastest and highest-fidelity gates is given in table II.

Experimental procedure

All gates were performed in a blade-type linear Paul trap^{38,39}, with axial centre-of-mass frequency $f_c = 1.92$ MHz for $t_g > 1 \mu\text{s}$, and $f_c = 1.86$ MHz for $t_g \leq 1 \mu\text{s}$ and for all single rectangular-pulse gates. The axial frequency was changed after re-aligning the Raman beams to suppress coupling to radial modes. In both cases the axial frequency was chosen such that the ion spacing was $12\frac{1}{2}\lambda_z$, where $\lambda_z = 283$ nm is the periodicity of the travelling standing wave providing the gate force. The gate was performed on the qubit states $|\downarrow\rangle = 4S_{1/2}|F = 4, M = +4\rangle$ and $|\uparrow\rangle = 4S_{1/2}|F = 3, M = +3\rangle$ in $^{43}\text{Ca}^+$ at $B = 14.6$ mT. (This value of the B -field gives access to the ‘‘atomic clock’’ qubit $|\downarrow'\rangle = 4S_{1/2}|F = 4, M = 0\rangle$ and $|\uparrow'\rangle = 4S_{1/2}|F = 3, M = +1\rangle$ with long coherence time, measured to be $T_2^* \sim 1$ minute in prior work², ideal for use as a memory qubit.) The ions were laser-cooled with dark-resonance Doppler cooling⁴⁰ to $\bar{n} \approx 1.8$ and further cooled with sideband cooling to $\bar{n} \lesssim 0.05$. After state preparation in $|\downarrow\downarrow\rangle$ we created an entangled state by placing the geometric phase-gate in one arm of a Ramsey interferometer split by a spin-echo π -pulse⁶. The gate errors were determined by using partial tomography⁴¹ to measure the fidelity of the created state with respect to the desired state $(|\downarrow\downarrow\rangle + |\uparrow\uparrow\rangle) / \sqrt{2}$.

Error analysis

All gate errors and fidelities quoted are after correction for state-preparation and readout errors³. The total state-preparation and readout error with two ions was typically $\bar{\epsilon}_{\text{SPAM}} = 1.4(1) \times 10^{-3}$ per ion (averaged over both qubit states). The 0.22(3)% error reported for the $t_g = 1.6 \mu\text{s}$ gate is the average of five experimental runs measured on two days. Directly after calibrating experimental parameters, the lowest error measured was 0.15(3)%; an hour



parameter	gate duration	
	$t_g = 483 \text{ ns}$	$t_g = 1.59 \mu\text{s}$
Raman detuning Δ	-200 GHz	-800 GHz
Raman beat note frequency ν	6.3802 MHz	2.6301 MHz
axial centre-of-mass frequency f_c	1.8615 MHz	1.9243 MHz
peak power (pulse-shaped beam)	192 mW	58 mW
power (non-shaped beam)	96 mW	48 mW
single-qubit phase $\phi_{\pi/2}$	91.4°	21.4°
pulse time t_1	71.4 ns	82.1 ns
pulse time t_2	64.5 ns	299.9 ns
pulse time t_3	46.7 ns	—
pulse time t_4	112.3 ns	819.5 ns
pulse fall-time t_f	5.0 ns	5.0 ns
pulse amplitude a_1	0.284	0.445
pulse amplitude a_2	0.617	0.838
pulse amplitude a_3	0.862	—
pulse amplitude a_4	1	1

TABLE II. (EXTENDED DATA) Gate parameters used for the fastest gate (7 segments) and for the highest-fidelity gate (5 segments). The pulse envelope above illustrates the definition of the pulse timing and amplitude parameters. The timing parameters refer to the timing of the waveform programmed into the AWG, for which a $t_f = 5.0 \text{ ns}$ rise/fall-time (0%–100%) was used; the measured rise/fall-time (10%–90%) of the laser pulses was 24 ns , due to the bandwidth of the particular AOMs used (see fig.2a). The waists ($1/e^2$ intensity radii) of the Raman beams were $33 \mu\text{m}$ and $38 \mu\text{m}$ for the pulse-shaped and non-shaped beams respectively.

after calibration, the measured error was 0.28(3)%. Quoted uncertainties are statistical only. We also measured the accumulated error for concatenated sequences of up to 7 gates, and found no evidence for coherent errors.

Errors due to radial mode excitation are largest for gates around $t_g = 800$ ns, because here the Raman beat note frequency ν is close to resonance with the radial mode frequencies (≈ 4.2 MHz); with our final Raman laser beam alignment we can limit errors due to radial mode excitation to $\epsilon_g < 5 \times 10^{-2}$ at $t_g = 800$ ns. An advantage of fast gates is that they are insensitive to errors associated with motional decoherence or heating; despite the relatively large heating rate of this trap ($\dot{\bar{n}} \approx 100 \text{ s}^{-1}$ for the axial centre-of-mass mode) the contribution to the gate error is negligible. A summary of the main errors present in our experiments, for the lowest-error gate, and for the fastest gate, is given in table I.

-
- ¹ D. J. Wineland *et al.*, Experimental Issues in Coherent Quantum-State Manipulation of Trapped Atomic Ions, *J.Res.NIST* **103**, 259 (1998).
- ² T. P. Harty *et al.*, High-Fidelity Preparation, Gates, Memory, and Readout of a Trapped-Ion Quantum Bit, *Phys.Rev.Lett.* **113**, 220501 (2014).
- ³ C. J. Ballance *et al.*, High-Fidelity Quantum Logic Gates Using Trapped-Ion Hyperfine Qubits, *Phys.Rev.Lett.* **117**, 060504 (2016).
- ⁴ J. P. Gaebler *et al.*, High-Fidelity Universal Gate Set for $^9\text{Be}^+$ Ion Qubits, *Phys.Rev.Lett.* **117**, 060505 (2016).
- ⁵ Q. A. Turchette *et al.*, Deterministic Entanglement of Two Trapped Ions, *Phys.Rev.Lett.* **81**, 3631 (1998).
- ⁶ D. Leibfried *et al.*, Experimental demonstration of a robust, high-fidelity geometric two ion-qubit phase gate, *Nature* **422**, 412 (2003).
- ⁷ J. Benhelm *et al.*, Towards fault-tolerant quantum computing with trapped ions, *Nat.Phys.* **4**, 463 (2008).
- ⁸ J. J. García-Ripoll, P. Zoller, and J. I. Cirac, Speed Optimized Two-Qubit Gates with Laser Coherent Control Techniques for Ion Trap Quantum Computing, *Phys.Rev.Lett.* **91**, 157901 (2003).
- ⁹ L.-M. Duan, Scaling Ion Trap Quantum Computation through Fast Quantum Gates,

- Phys.Rev.Lett. **93**, 100502 (2004).
- ¹⁰ J. J. García-Ripoll, P. Zoller, and J. I. Cirac, Coherent control of trapped ions using off-resonant lasers, Phys.Rev.A **71**, 062309 (2005).
- ¹¹ A. M. Steane *et al.*, Pulsed force sequences for fast phase-insensitive quantum gates in trapped ions, New J.Phys. **16**, 053049 (2014).
- ¹² M. Palmero *et al.*, Fast phase gates with trapped ions, Phys.Rev.A **95**, 022328 (2017).
- ¹³ J. J. Bollinger *et al.*, A 303-MHz Frequency Standard Based on Trapped Be⁺ Ions, IEEE Trans.Instr.Meas. **40**, 126 (1991).
- ¹⁴ Y. Wang *et al.*, Single-qubit quantum memory exceeding 10-minute coherence time, ArXiv (2017), arXiv:1701.04195.
- ¹⁵ D. L. Moehring *et al.*, Entanglement of single-atom quantum bits at a distance, Nature **449**, 68 (2007).
- ¹⁶ R. Barends *et al.*, Superconducting quantum circuits at the surface code threshold for fault tolerance, Nature **508**, 500 (2014).
- ¹⁷ M. Veldhorst *et al.*, A two-qubit logic gate in silicon, Nature **526**, 410 (2015).
- ¹⁸ A. G. Fowler *et al.*, Surface codes: Towards practical large-scale quantum computation, Phys.Rev.A **86**, 032324 (2012).
- ¹⁹ C. Monroe and J. Kim, Scaling the Ion Trap Quantum Processor, Science **339**, 1164 (2013).
- ²⁰ M. H. Devoret and R. J. Schoelkopf, Superconducting Circuits for Quantum Information: An Outlook, Science **339**, 1169 (2013).
- ²¹ Y. Lin *et al.*, Sympathetic Electromagnetically-Induced-Transparency Laser Cooling of Motional Modes in an Ion Chain, Phys.Rev.Lett. **110**, 153002 (2013).
- ²² R. Bowler *et al.*, Coherent Diabatic Ion Transport and Separation in a Multizone Trap Array, Phys.Rev.Lett. **109**, 080502 (2012).
- ²³ T. Ruster *et al.*, Experimental realization of fast ion separation in segmented Paul traps, Phys.Rev.A **90**, 033410 (2014).
- ²⁴ R. Noek *et al.*, High speed, high fidelity detection of an atomic hyperfine qubit, Opt.Lett. **38**, 4735 (2013).
- ²⁵ Q. A. Turchette *et al.*, Decoherence and decay of motional quantum states of a trapped atom coupled to engineered reservoirs, Phys.Rev.A **62**, 053807 (2000).
- ²⁶ T. Ruster *et al.*, A long-lived Zeeman trapped-ion qubit, App.Phys.B **122**, 254 (2016).

- ²⁷ R. Ozeri *et al.*, Errors in trapped-ion quantum gates due to spontaneous photon scattering, *Phys.Rev.A***75**, 042329 (2007).
- ²⁸ M. J. McDonnell *et al.*, Long-lived mesoscopic entanglement outside the Lamb-Dicke regime, *Phys.Rev.Lett.* **98**, 063603 (2007).
- ²⁹ P. O. Schmidt *et al.*, Spectroscopy Using Quantum Logic, *Science* **309**, 749 (2005).
- ³⁰ V. Meyer *et al.*, Measurement of the 1s-2s Energy Interval in Muonium, *Phys.Rev.Lett.* **84**, 1136 (2000).
- ³¹ S. Machnes *et al.*, Superfast Laser Cooling, *Phys.Rev.Lett.* **104**, 183001 (2010).
- ³² V. M. Schäfer *et al.*, Optical injection and spectral filtering of high-power ultraviolet laser diodes, *Opt.Lett.* **40**, 4265 (2015).

-
- ³³ Ti:sapphire laser, M-Squared SolsTiS ECD-X.
- ³⁴ AOM, Brimrose CQM-200-40-.400/OW.
- ³⁵ AWG, Agilent N8241A, 1.25 GHz clock rate, 15 bits vertical resolution.
- ³⁶ DDS, Enterpoint Milldown card, 200 MHz.
- ³⁷ C. Degenhardt *et al.*, Influence of chirped excitation pulses in an optical clock with ultracold calcium atoms, *IEEE Trans.Instr.Meas.* **54**, 771 (2005).
- ³⁸ S. T. Gulde, Ph.D. thesis, University of Innsbruck (2003).
- ³⁹ S. R. Woodrow, M.Sc. thesis, University of Oxford (2015).
- ⁴⁰ D. T. C. Allcock *et al.*, Dark-resonance Doppler cooling and high fluorescence in trapped Ca-43 ions at intermediate magnetic field, *New J.Phys.* **18**, 023043 (2016).
- ⁴¹ C. A. Sackett *et al.*, Experimental entanglement of four particles, *Nature* **404**, 256 (2000).
- ⁴² The minimum gate time given in ref.³, $3.8 \mu\text{s}$, is the fwhm of the laser pulse; for fair comparison with the gates reported in the present work we quote the total gate time from the start of the rising edge to the end of the falling edge, which was $5.3 \mu\text{s}$.
- ⁴³ A demonstration of the method proposed in ref.⁸ has very recently been reported (J. D. Wong-Campos *et al.*, arXiv:1709.05179), with gate time $t_g = 18.5 \mu\text{s} \approx 23/f_c$.

ACKNOWLEDGEMENTS

This work was supported by the U.K. EPSRC “Networked Quantum Information Technologies” Hub, and the U.K. Defence, Science and Technology Laboratory. VMS acknowledges funding from Balliol College, Oxford. CJB acknowledges funding from Magdalen College, Oxford. We thank S. R. Woodrow for her work on the trap design, T. P. Harty for contributions to the apparatus, and acknowledge the use of the University of Oxford Advanced Research Computing facility (doi:10.5281/zenodo.22558). The experiments benefitted from the use of the ARTIQ control system (doi:10.5281/zenodo.591804).

AUTHOR CONTRIBUTIONS

CJB performed the numerical modelling. VMS and CJB designed and performed the experiments. KT built the ion trap and characterized the fast acousto-optic modulators. LJS and TGB built optical and control systems. VMS, CJB, AMS and DML wrote the manuscript, which all authors discussed.

AUTHOR INFORMATION

The authors declare no competing financial interests. Correspondence and requests for materials should be addressed to DML (d.lucas@physics.ox.ac.uk).

DATA AVAILABILITY

The data that support the plots within this paper and other findings of this study are available from the corresponding author upon reasonable request.